Nationaal Lucht- en Ruimtevaartlaboratorium

National Aerospace Laboratory NLR

NLR-TP-2012-486

Reformulation of a three-dimensional inverse design method for application in a high-fidelity computational fluid dynamics environment

M.P.C. van Rooij and A.J. Medd

Nationaal Lucht- en Ruimtevaartlaboratorium
National Aerospace Laboratory NLR

Executive summary

Reformulation of a three-dimensional inverse design method for application in a high-fidelity computational fluid dynamics environment

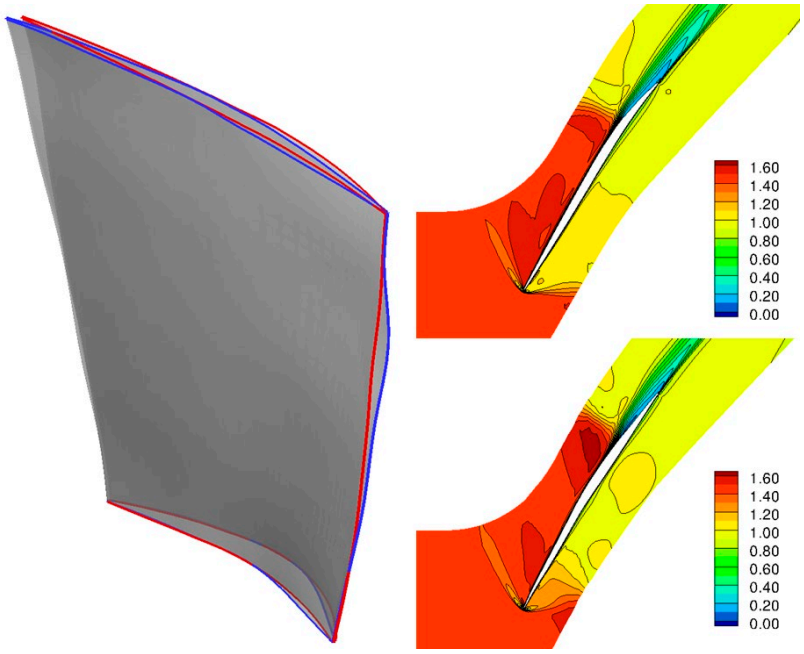

Report no.
NLR-TP-2012-486

Author(s)
M.P.C. van Rooij
A.J. Medd

Report classification
UNCLASSIFIED

Date
March 2013

Knowledge area(s)
Computational Physics en theoretische aërodynamica
Gasturbinetechnologie
Computational Mechanics and Simulation Technology

Descriptor(s)
Inverse design
CFD (Computational Fluid Dynamics)
Gas Turbine Technology
Compressor

Problem area

Current turbo machinery design systems increasingly rely on multistage CFD as a means to diagnose designs and assess performance potential. However, design weaknesses attributed to improper stage matching are addressed using often ineffective strategies involving a costly iterative loop between blading modification, revision of design intent, and further evaluation of aerodynamic performance.

Three-dimensional inverse design has been shown to be a reliable and powerful tool for facilitating the refinement of blading design and improving stage matching, thereby providing increased aero-design quality and productivity in difficult design situations. However, inverse design has not been incorporated widely into design systems.

Reasons for this may be that many inverse techniques are limited to two dimensional problems, or are

This report is based on a presentation held at the ASME Turbo Expo, Copenhagen (Denmark), June 15-18, 2012.

highly integrated with a specific flow solver and therefore difficult to integrate with proprietary or commercial CFD methods.

Description of work
A reformulation of a three-dimensional inverse design method is presented here that overcomes these limitations. The inverse method has been separated from the flow solver, and is now purely a geometry modifier. Camber modification is performed using a blade velocity derived from the difference between prescribed and actual pressure loading.

The developed inverse design method is demonstrated through redesign and subsequent recovery of a highly loaded, high speed rotor blade with regions of separated flow.

Results and conclusions
The new method is fully consistent with viscous flow modeling, and completely eliminates differences between analysis and inverse calculations.

Because the reformulation has decoupled the inverse method from the flow solver, it is possible to supplement any CFD-code with the developed inverse design module, provided an interface can be created between the solver and the inverse module through which to pass information on flow and mesh. This makes inverse design available to most design offices.

Applicability
The new inverse method has been tested successfully for redesign of axial and centrifugal compressor blading. The method needs to be tested before application on turbine blading.

Nationaal Lucht- en Ruimtevaartlaboratorium, National Aerospace Laboratory NLR

Anthony Fokkerweg 2, 1059 CM Amsterdam,
P.O. Box 90502, 1006 BM Amsterdam, The Netherlands
Telephone +31 88 511 31 13, Fax +31 88 511 32 10, Web site: www.nlr.nl

Nationaal Lucht- en Ruimtevaartlaboratorium
National Aerospace Laboratory NLR

NLR-TP-2012-486

Reformulation of a three-dimensional inverse design method for application in a high-fidelity computational fluid dynamics environment

M.P.C. van Rooij and A.J. Medd[1]

[1] Honeywell Aerospace

This report is based on a presentation held at the ASME Turbo Expo, Copenhagen (Denmark), June 15-18, 2012.

Customer	National Aerospace Laboratory NLR
Contract number	-----
Owner	NLR
Division NLR	Aerospace Vehicles
Distribution	Unlimited
Classification of title	Unclassified
	March 2013

Approved by:

Author	Reviewer	Managing department
M.P.C. van Rooij	B.I. Soemarwoto	K.M.J. de Cock
MvR		
Date: 27-03-2013	Date: 28-03-2013	Date: 29-03-2013

Summary

Three-dimensional inverse design has been shown to be a reliable and powerful tool for facilitating the refinement of blading design and improving stage matching, thereby providing increased aero-design quality and productivity in difficult design situations. However, inverse design has not been incorporated widely into design systems. Reasons for this may be that many inverse techniques are limited to two dimensional problems, or are highly integrated with a specific flow solver and therefore difficult to integrate with proprietary or commercial CFD methods.

A reformulation of a three-dimensional inverse design method is presented here that overcomes these limitations. The new method is fully consistent with viscous flow modelling. Camber modification is performed using a blade velocity derived from the difference between prescribed and actual pressure loading. The new inverse method completely eliminates differences between analysis and inverse calculations.

Moreover, the reformulation effectively decouples the inverse method from the flow solver. This makes it possible to supplement any CFD-code with the developed inverse design module, provided an interface can be created between the solver and the inverse module through which to pass information on flow and mesh. This makes inverse design available to most design offices.

This page is intentionally left blank.

Contents

Abbreviations

A	area
c	speed of sound
f	wrap angle/camber (circumferential coordinate)
n	surface normal
p	static pressure
r	radial coordinate/direction
T	temperature
t	time
V	absolute velocity
W	relative velocity
z	axial coordinate/direction
θ	blade surface (circumferential coordinate)
ρ	density
LE	leading edge
TE	trailing edge
M	mass flow

subscripts

0	total condition
b	outlet/back
ba	blade axis/stacking line
i	index
n	normal
$spec$	specified
θ	circumferential coordinate/direction

superscripts

+	upper blade surface
-	lower blade surface

1 Introduction

Computational Fluid Dynamics (CFD) has become an indispensable tool for aerodynamic design of turbo machinery blading. Multistage CFD methods are very well suited for diagnosing design shortcomings that adversely impact performance and operability. In the design process, simulation results are routinely used to improve performance deficiencies and revise aerodynamic matching conditions. However, while CFD analysis can diagnose shortcomings in blading design, they do not offer an effective means for design adjustments, especially for advanced designs.

Inverse methods have been shown to be powerful and reliable tools for facilitating the refinement of blading design. Their main strength lies in the direct control offered over local aerodynamics and, when the method is based on pressure loading, net circulation. Recent application examples of three-dimensional inverse methods are provided by Ji et al. [9] and Mileshin et al. [3]. Van Rooij et al. [7,8] and Hield [1] developed multistage methods and demonstrated their ability to significantly simplify the process of stage matching.

Nevertheless, inverse methods have not yet gained wide acceptance in design offices. Two main reasons might account for this. First, most of the published inverse methods are limited to two-dimensional problems. Second, inverse methods are often highly integrated with a specific flow solver due to a special boundary condition or time-accurate formulation, which makes them difficult to integrate with proprietary or commercial CFD methods. An example of such a special boundary treatment is the transpiration technique, in which the blade wall boundary conditions are formulated so that the flow is allowed to cross the wall boundary with finite magnitude. During the design calculation, the wall velocity is modified based on the prescribed blade surface pressure or pressure loading, and the blade shape is aligned to the evolving velocity field. A relatively large velocity at the blade surface is required, with Y+-values of 30-100 in near-wall cells. This precludes the use of inverse design in a high-fidelity flow analysis environment, where Y+ is typically driven towards 1 in order to obtain satisfactory boundary layer resolution. Differences in flow field prediction between the inverse method and high-fidelity analysis can become unacceptably large, especially when dealing with highly loaded and transonic blading. Application of the inverse method then becomes impractical at best.

Several recent publications have described inverse methods that do not rely on the transpiration technique, e.g. Hield [1], Daneshkhah and Ghaly [2] and Mileshin et al. [3]. All three adjust the blade camber based on a virtual blade velocity, which is derived from the difference between prescribed and actual pressure loading. Hield's method is embedded in a lower-fidelity time-

marching quasi-steady 3D solver employing a sheared H-mesh and a simple mixing-length turbulence model, though it theoretically could be used with a more sophisticated flow solver. Both Daneshkhah and Ghaly, and Mileshin use a time-accurate formulation to improve robustness and convergence speed, and therefore are highly integrated with the flow solver formulation.

An inverse design method is presented here that addresses all of the limitations raised above. It is a reformulation of the inverse method used in the inverse design code INV3D developed at Syracuse University. Camber modification is no longer performed by tracing the velocity field. Instead, the camber is adjusted based on a blade velocity derived from the difference between prescribed and actual pressure loading. Thus, it does not rely on an "inverse" blade wall boundary condition, and a conventional "no-slip" condition can be used instead. This fully eliminates the residual mass flow through the blade surface, and makes the method consistent with viscous flow modelling.

As a result of the reformulation, the inverse design method has become a separate module that performs geometry modification only and exists next to the flow solver. Potentially, any CFD code can be supplemented with the described inverse design module provided an interface can be created between the solver and the inverse module through which to pass flow and mesh information.

In the following sections, the inverse method in the original INV3D code is discussed, followed by a description of the reformulated method. Results of design exercises will be provided demonstrating the ability of the inverse method to reproduce a target pressure loading. Finally, conclusions on the presented work will be given.

2 Method Description

2.1 Original inverse method INV3D

The development of the inverse design code INV3D has been reported in previous publications by Dang [4] , Damle et al. [5] , Medd at al. [6] , Van Rooij et al. [7] ,[8] , Ji et al. [9] and Qiu et al. [10] . The latter gives a detailed description of the inverse boundary condition and camber-construction technique that were used. The method has been applied successfully to the redesign of highly loaded transonic blading (Larosiliere et al. [11] and Van Rooij et al. [7] ,[8]).

The computational method solves the three-dimensional Reynolds-Averaged Navier-Stokes (RANS) equations in a cylindrical z,r,θ-coordinate system on a simple straight H-mesh using the finite-volume time-marching cell-centered scheme of Jameson et al. [11] . It employs a four-stage Runge-Kutta time integration scheme. Use of residual smoothing [12] ,[13] allow the code to be run routinely at a CFL number of 5. Inlet and exit boundary conditions are non-reflective. Boundary layers are assumed turbulent and turbulence effects are modelled with an adaptation of the Baldwin-Lomax turbulence model [15] using wall functions if the near wall Y^+-value exceeds 11.06. Tip gap leakage flows are approximated by assuming periodicity across the extended blade surfaces in the clearance gap.

In inverse mode, the primary prescribed quantities are the definition of blade axis or stacking line in terms of its axial grid-line location i_{ba} and tangential orientation along the camber surface $f_{ba}(r)$, the blade thickness distribution $T(z,r)$, and the pressure loading distribution $\Delta p(z,r)$. The blade axis provides a reference for locating the various spanwise blade sections in space and thus must be compatible with the spanwise distribution of Δp. The pressure loading is related to mass flow and flow turning, as is reflected in the angular momentum-force balance relationship for a quasi-3D blade element:

$$\int_{LE}^{TE} r\,\Delta p\,dA_\theta \approx \dot{m}\left[\left(r\bar{V}_\theta\right)_{TE} - \left(r\bar{V}_\theta\right)_{LE}\right] \tag{1}$$

In the above relation, Δp is the difference between the blade upper and lower surface pressures at fixed axial locations; the subscripts LE and TE denote leading and trailing edges, respectively, $\dot{m}$ is the mass flow rate, A_θ is the projected surface area in the tangential direction, and $r\bar{V}_\theta$ is the mass-averaged swirl velocity. For a given set of inputs, the three-dimensional inverse method computes the corresponding wrap angle $f(z,r)$. Thus, it is a semi-inverse procedure in the sense that the full geometry is not evolved and only the mean camber surface $f(z,r)$ is adjusted.

The velocity at the blade surface required to obtain the specified pressure loading is obtained from the following compatibility equation [10] :

$$W^{+}_{n,new} = W^{-}_{n,new} = \frac{\Delta p_{spec} - (p^{+} - p^{-}) + \rho^{+} c^{+} W^{+}_{n} + \rho^{-} c^{-} W^{-}_{n}}{\rho^{+} c^{+} + \rho^{-} c^{-}} \quad (2)$$

The computed blade normal velocities are used to update the ghost cell values along the blade surface to enforce $W_{n,new}$. Equation (2) is therefore also referred to as inverse boundary condition. A camber-construction technique is used to align the blade with the velocity field at the blade surface, which originally consisted of an implicit Crank-Nicholson scheme. Mesh-deformation is not accounted for in the flow solver. In order to prevent convergence problems because of this, the camber is typically updated every 5-10 iterations to allow for the flow to stabilize between camber updates.

Several modifications were made to this basic methodology in order to make it more robust and produce smoother blade geometries. These can be summarized as (1) camber generation using a non-uniform rational B-spline (NURBS) surface based minimization method to handle (mild) tip clearance flows and ensure blade smoothness, and (2) exclusion of parts of the blade from the inverse scheme, such as leading and trailing edges for better geometric fidelity [6] , and the hub and tip regions for increased robustness against strong three-dimensional flows [8] . Another modification was proposed by Ji [9] , who successfully performed inverse design of a centrifugal compressor with associated strong three-dimensional flow field, by applying the inverse method to two or three blade sections only and obtaining the full camber surface by interpolation and extrapolation from these sections.

The implementation of these modifications gradually led to the release of target loading shape as absolute design goal in favor of blade smoothness and method robustness. Another consequence was an increase in the difference between results of the design and subsequent analysis calculations, since the prescribed loading calculation was enforced through the inverse boundary condition Eqn. (2) during the design calculation.

2.2 Reformulated inverse method

2.2.1 Overall inverse design process

Based on the observations above, a reformulation of the inverse method was defined. The main requirements were that it (1) work without special inverse boundary conditions and/or aspiration technique; (2) be compatible with arbitrary mesh topologies; and (3) be separated from the flow solver. Based on the work by Ji [9] , it was furthermore opted to specify pressure loading and perform inverse-driven camber modification on a few blade sections instead of the full blade surface, and treat these inverse sections as isolated, quasi-3D blade elements. This makes it possible to exclude from the inverse design process, blade sections with large regions of separated flow or strong three-dimensional surface flows.

The developed inverse design process is shown in Figure 1. After the mesh and flow solution are transferred from the flow solver to the inverse module, the geometry and near-wall flow field are interpolated onto a uniform mesh in the meridional (z,r) plane, hereafter designated inverse mesh. This interpolation is necessary because of the tangential formulation of the inverse method, which requires the flow variables and geometry coordinates along the upper and lower blade surfaces to be at identical z,r-coordinates. From the interpolated upper and lower blade surfaces, the tangential camber surface $f(z,r)$ is readily computed:

$$f = \tfrac{1}{2}\left(\theta^{+} + \theta^{-}\right) \tag{3}$$

The pressure and density fields on the blade surfaces are also interpolated onto the inverse mesh. The inverse mesh consists of 101 by 101 points, each cell thus measuring 1% chord by 1% span. At this resolution, very good preservation of the calculated blade pressure distribution is obtained, also around shocks. A uniform mesh is used because of the camber smoothing described below.

At the user-defined inverse sections, a normal velocity $W_{n,new}$ is defined based on the difference between the prescribed and actual pressure loadings. Using this normal velocity, the camber at these sections is modified. The exact procedure is explained in detail in 2.2.2. Regions near the leading and trailing edge are usually excluded from this procedure because large gradients in pressure loading at these locations may induce waviness in the blade shape if not carefully defined in the prescribed loading. These regions usually measure 2-5% chord. In this case, the camber is extrapolated by a first-order method to the blade edges.

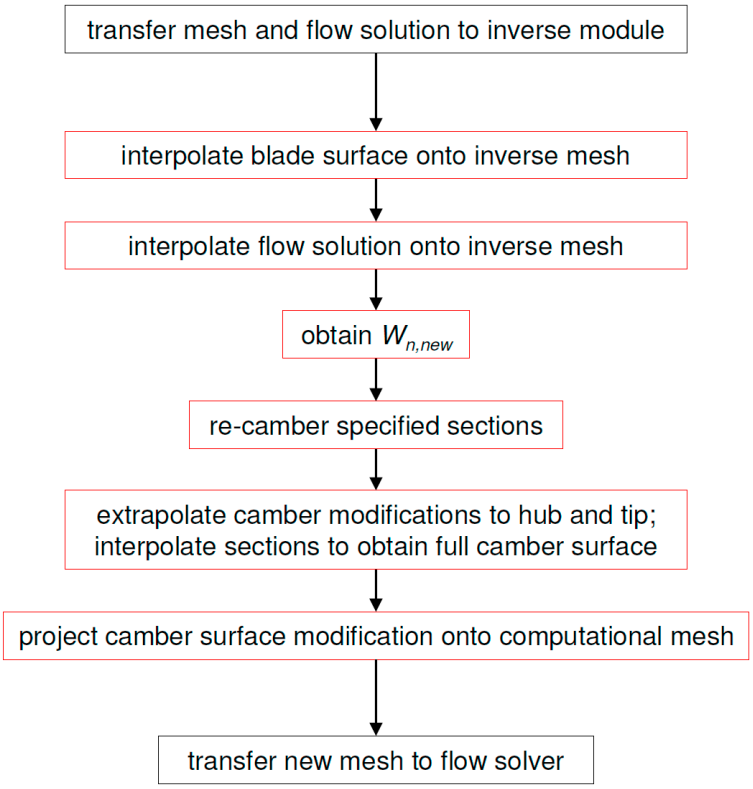

Figure 1 Inverse design process. Items in red are part of the new inverse design module

The obtained camber lines are then fitted with a NURBS curve [12] to ensure smoothness. The number of control points normally ranges from 5 to 15. The higher the number of control points, the more detail in the camber line is preserved and the more exact a prescribed pressure loading distribution is achieved. The fitting algorithm distributes the control points based on the distribution of the data points to be fitted. Clustering of data points on a curve segment would result in corresponding clustering of the control points near this segment. As a result, more detail is preserved at this curve section at the expense of the remainder of the curve. Since this is undesirable for camber smoothing, a uniform inverse mesh is used.

If the hub and/or tip sections are not included in the set of inverse sections, modifications to their respective camber lines are obtained by extrapolation from the nearest section. The complete blade surface is constructed through interpolation of the modified sections in the radial direction. Finally, the changes in camber are mapped onto the computational mesh, which is then transferred to the flow solver. Mesh points are moved in the tangential direction only, and the complete mesh domain is modified. Because camber modifications are typically small with respect to the blade spacing, the induced mesh deformations have only a minor impact on mesh quality.

2.2.2 Inverse method details

In the original INV3D inverse method, the compatibility equation (2) was used to enforce the pressure loading through adjustment of the velocity on the blade surface. In the present method, a different approach is taken. In order to be fully consistent with viscous flow modelling, the inverse method needs to be able to derive a modified camber surface with the condition that the normal velocity on the blade surfaces

$$W_n^+ = W_n^- = 0 \tag{4}$$

This is done as follows. With condition (4), the compatibility equation (2) becomes

$$W_{n,new} = \frac{\Delta p_{spec} - (p^+ - p^-)}{\rho^+ c^+ + \rho^- c^-} \tag{5}$$

where the pressure p, density ρ and speed of sound c are obtained from the flow solution supplied by the flow solver. The obtained normal velocity is now interpreted as the velocity with which the blade, or more specifically camber, needs to deform locally in order to produce the specified pressure loading. This is analogous to the methods described by e.g. Hield [1] and Daneshkhah and Ghaly [2] . Since each inverse section is treated as an isolated, quasi-3D blade element and camber movement is restricted to the circumferential direction, the local change in wrap angle is

$$\Delta f = \Delta t \cdot W_{n,new} \cdot n_\theta \tag{6}$$

where Δt is a pseudo-time step and $n_\theta = \frac{1}{2}(n_\theta^+ + n_\theta^-)$ the average circumferential component of the blade surface normal. The change in camber Δf is calculated for each point (i,j) on the inverse mesh, where index i identifies the chordwise location on the inverse grid and index j the spanwise location. The new camber line at section j is then obtained by integrating Δf upstream and downstream from the blade axis located at i_{ba}. Integration in the upstream direction gives

$$f_{i,j}^{new} = f_{i,j}^{old} - \sum_{in=i_{ba}-1}^{i} \Delta f_{in,j} \tag{7}$$

and integration downstream

$$f_{i,j}^{new} = f_{i,j}^{old} + \sum_{in=i_{ba}+1}^{i} \Delta f_{in,j} \tag{8}$$

as illustrated in Figure 2. Through numerical experimentation, a suitable value for the pseudo-time step used for camber modification has been established to be:

$$\Delta t = 0.01 \tag{9}$$

A user-definable relaxation factor is added, which is normally set to:

$$\xi = 0.2 \tag{10}$$

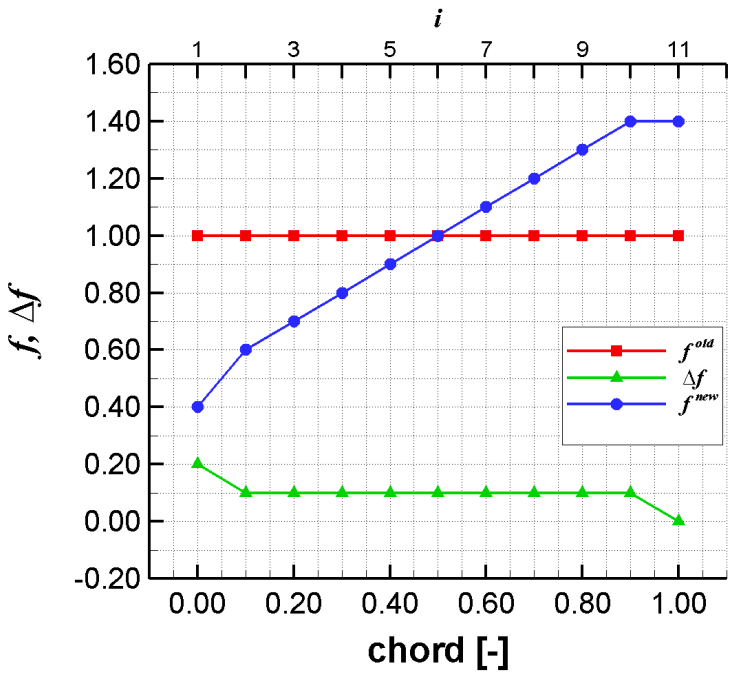

Figure 2 Illustration of camber line modification using Eqns. (7) and (8). In this example, the blade axis is located at 50% chord

3 Demonstration of developed inverse method

The reformulated inverse method was attached to a modified flow solver from the original INV3D code described above. The new solver incorporates many core algorithms of the original, but contains some simplifications and extensions. For instance, the "viscous slip" wall boundary condition has been removed, while the capability to handle mesh types other than straight H-mesh as well as multi-block grids has been added. Improvements to the turbulence model were intended but had not been realized at the time of writing this paper. The new solver is parallelized using OpenMP [20].

The improvements in predictive accuracy realized by the solver modifications are demonstrated on NASA Rotor 37. Discussions of CFD modelling of Rotor 37 can be found in e.g. [16-18]. The computational mesh consists of four blocks: H-type inlet and outlet blocks, a C-mesh around the blade and an O-mesh in the tip clearance gap (Figure 3). The cell counts of the mesh blocks are listed in Table 1.

Figure 4 shows the circumferentially mass-averaged total pressure distribution at the outlet. Results obtained with INV3D on a straight H-mesh and with "slip" wall boundary condition, and experimental results are included as well. The improvements to the solver have resulted in a much better agreement with the experimental results. The total pressure deficit near the hub is not fully captured, but this is in line with other published CFD results [16-18]. This deficit might (in part) be caused by hub leakage as reported in [19]. Predictive accuracy is expected to improve further with upgrade of the turbulence model. Contours of relative Mach numbers at 90% span are shown in Figure 5. The flow is characterized by high Mach number and strong shock-boundary layer interaction resulting in flow separation at approximately 70% chord. Flow separation, either shock-induced or resulting from over-turning, is present along the entire blade span, as can be seen in Figure 6.

Table 1 Mesh type and cell count of the four mesh blocks

block name	type	i-cells (axial)	j-cells (radial)	k-cells (pitchwise)
inlet	*H*	20	62	20
blade passage	*C*	160	62	34
tip clearance	*O*	120	6	5
outlet	*H*	20	62	68

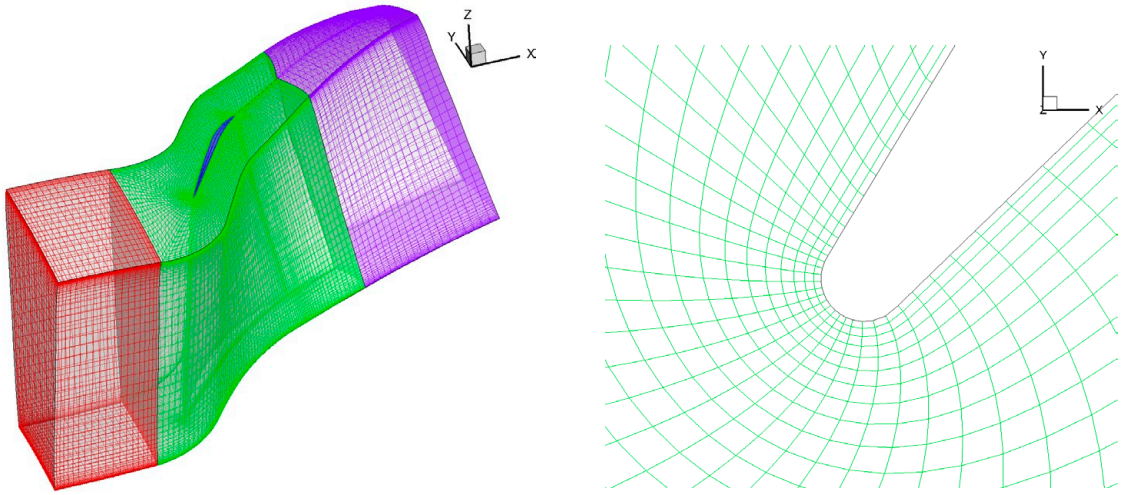

Figure 3 *Computational mesh used in the calculations. Left: HCH mesh around Rotor 37 with O-mesh in tip clearance. Right: detailed view of the mesh around the leading edge*

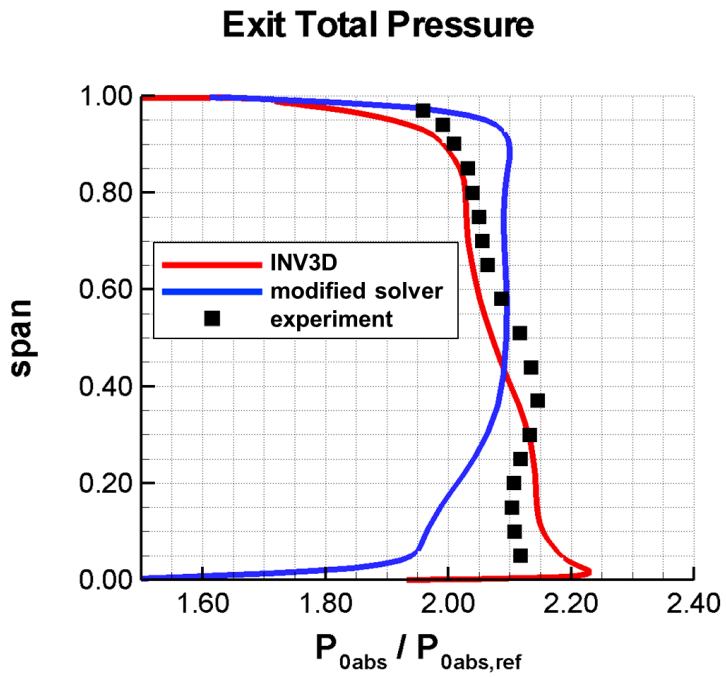

Figure 4 *Comparison of CFD analysis result using INV3D (previous inverse code with "slip" wall boundary condition), the modified solver from INV3D used with the reformulated inverse method, and experimental data [15]. CFD calculations at p_b=1.20*

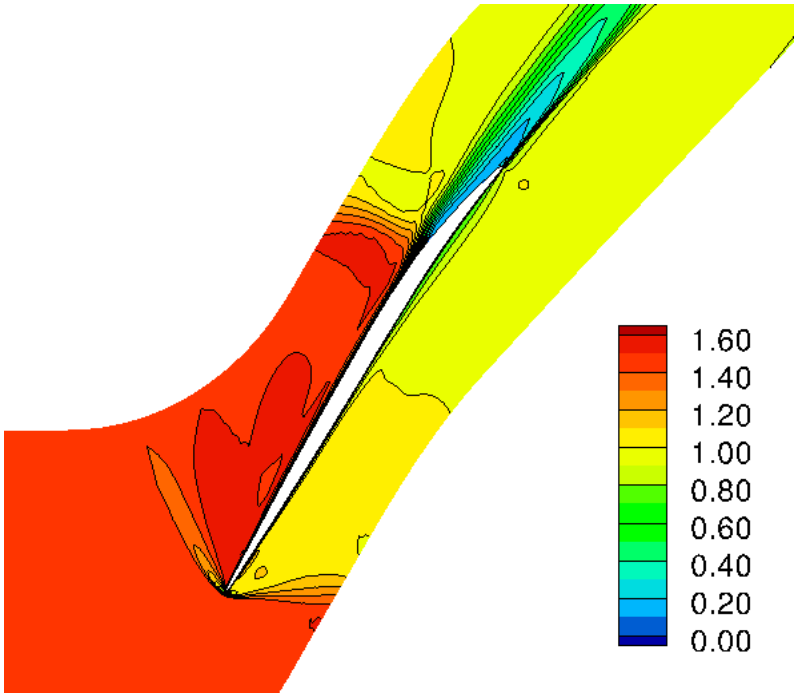

Figure 5 Contours of relative Mach number at 90% span. Original geometry, p_b=1.20

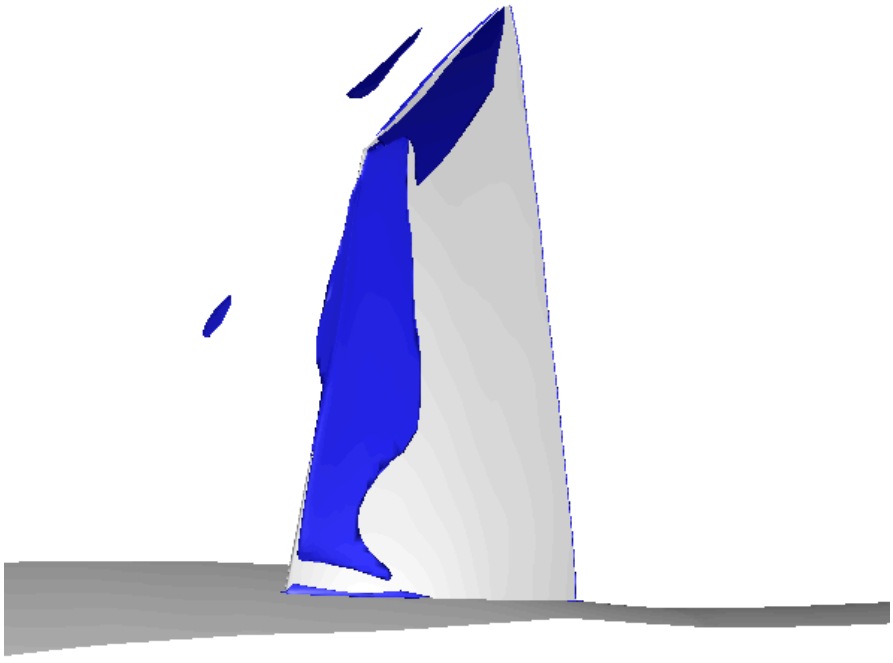

Figure 6 Regions of reversed flow (negative axial velocity). View of blade suction side; flow direction from right to left

3.1 Redesign demonstration

A redesign exercise is performed on Rotor 37 to demonstrate the ability of the new inverse method to produce a target pressure loading. Rotor 37 is selected for this demonstration because of the challenging conditions it poses for a design method, namely high loading, high Mach numbers with strong shock-boundary layer interaction and separated flow present along the span from approximately 70% chord to the trailing edge, as illustrated in Figure 5.

Five design stations are selected, located at 10%, 30%, 50%, 70% and 90% span. The specified loading shapes at these sections are shown in Figure 7, together with the loading shapes produced by the original geometry. Overall, the objective of the redesign can be summarized as decreased incidence, decreased loading on the aft section of the blade, and swallowed shock at all blade sections. Note that the purpose of this exercise is to demonstrate the ability of the inverse method to produce the prescribed loading shapes, not to obtain improved performance. The stacking line or blade axis was placed at 40% chord. Sections of 5% chord at the leading and trailing edges were excluded from the inverse procedure. A NURBS curve of ten control points and degree two was used to smooth the obtained blade sections.

The design calculation was started using the previous analysis result as initial solution and run for 2,000 iterations, with camber updated every ten iterations. The convergence history of camber and flow are shown in Figure 8 and Figure 9, respectively. Convergence of camber was reached near the end of the calculation. The flow reached its steady state solution after approximately 1,000 iterations. Upon inspection of the convergence plots, it is clear that already after fifty camber updates a blade shape is obtained with an overall performance close to the final solution.

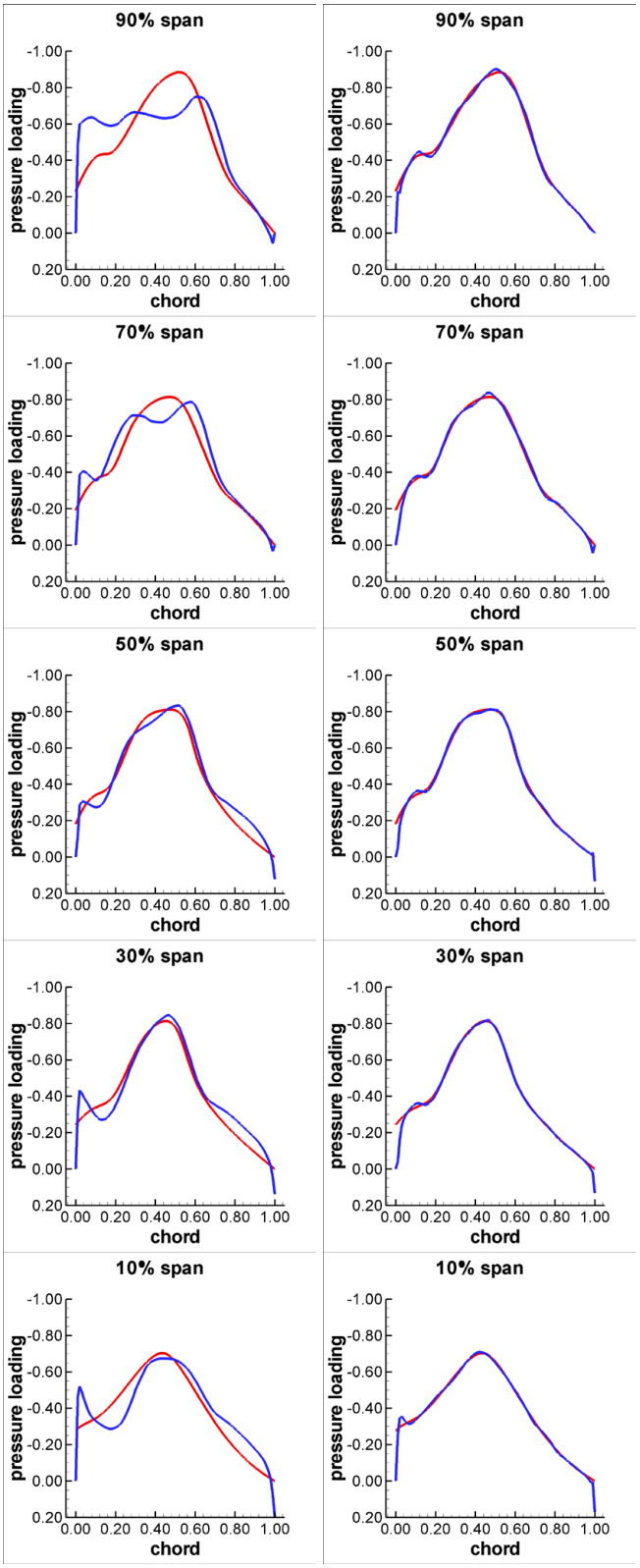

Figure 7 Comparison between prescribed loading (red) and actual loading (blue) at start of design calculation (left) and end of design calculation (right)

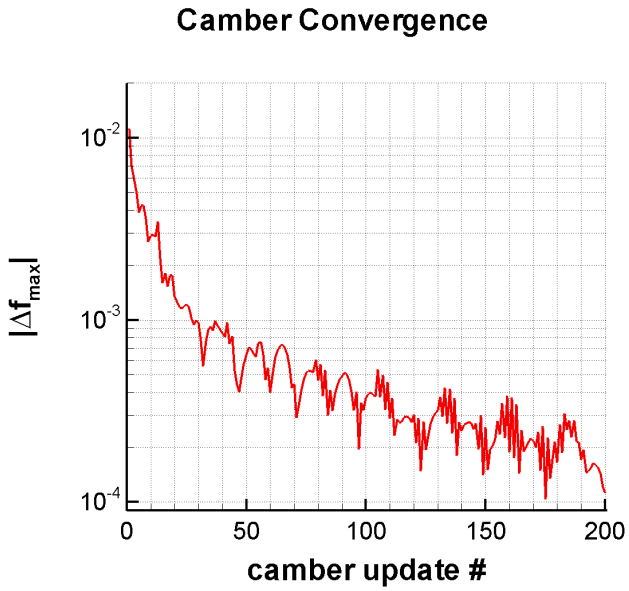

Figure 8 Convergence of camber during design calculation. The camber was updated every 10 solver iterations

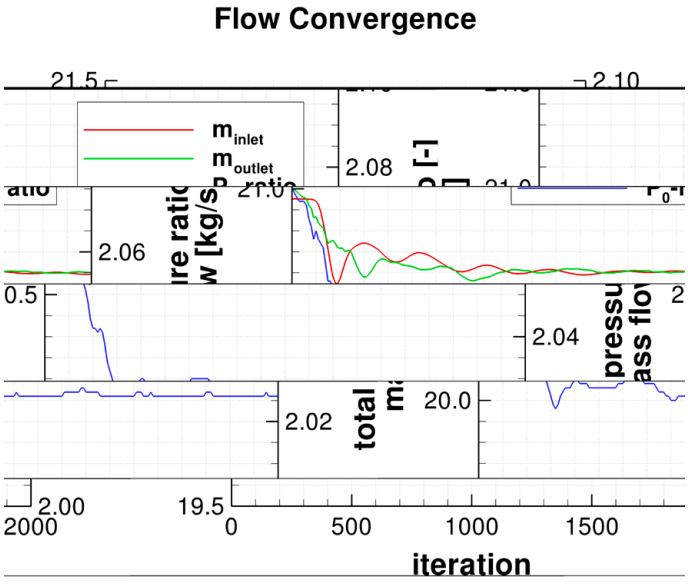

Figure 9 Convergence of flow in terms of overall performance parameters during design calculation

Figure 7 shows a comparison of the prescribed and obtained loading shapes at the design sections. The prescribed loading shapes are matched very closely. In certain regions, most notably the leading and trailing edges and the shock, the obtained loading shows minor oscillations around the smooth prescribed curves. This is a result of the camber smoothing, which removes minor kinks and fluctuations from the camber. The smoothed blade does not support the smooth loading distribution. A more exact agreement with the prescribed loading shape can be achieved by increasing the number of NURBS control points used to fit the camber line.

Figure 10 shows a blade-to-blade view showing contours of relative Mach numbers at 90% span. In agreement with the design objective at this section, the shock is located within the blade passage. A three-dimensional view of the original and redesigned blade is given in Figure 11. Blade sections at 10% and 70% span are shown in Figure 12. The desired reduction in incidence has resulted in an obvious change in metal angle between 50% and 100% span. The overall performance of the redesigned blade is a mass flow of 20.6 kg/s, a total pressure ratio of 2.026 and adiabatic efficiency of 88.8%.

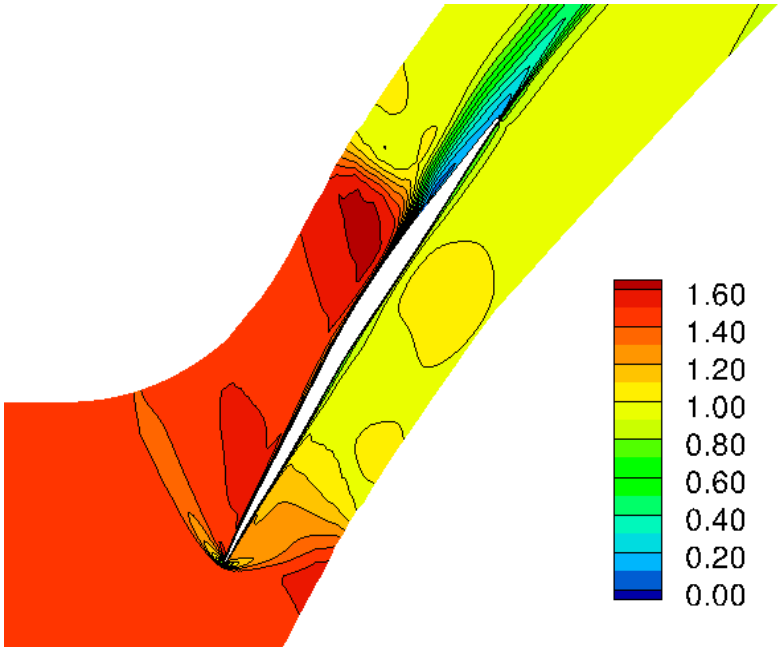

Figure 10 Contours of relative Mach number at 90% span. Redesign geometry, p_b=1.20

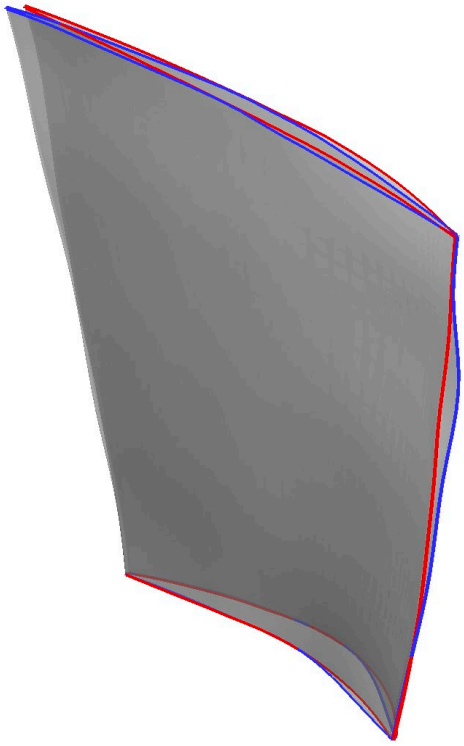

Figure 11 Comparison of original (red) and redesign (blue) geometries. View on trailing edge/pressure side

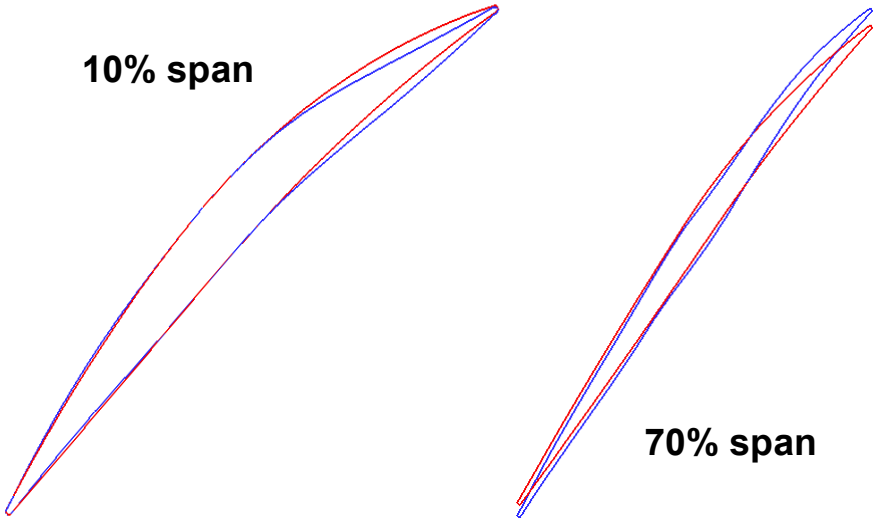

Figure 12 Comparison of original (red) and redesign (blue) geometries at 10% and 70% span

3.2 Recovery demonstration

As a final test of the new inverse method presented here, a recovery exercise is performed. The result from the previous redesign exercise is the starting point for a design calculation with the pressure loading produced by the original Rotor 37 blade as design input. Upon convergence, the resulting blade must match the original blade both in shape and in performance.

As for the redesign exercise, the design blade sections are at 10%, 30%, 50%, 70% and 90% span. All other design parameters are also identical to those used in the redesign exercise above. Figure 13 shows blade sections at 10% and 70% span for the original and recovered geometries. The original geometry is reproduced closely. Minor deviations exist, e.g. at the trailing edge at 70% span. These can be attributed to the presence of separated flow and camber line smoothing. The overall performance numbers of the original and recovered geometries are listed in Table 2. The performance of the original geometry is matched almost exactly.

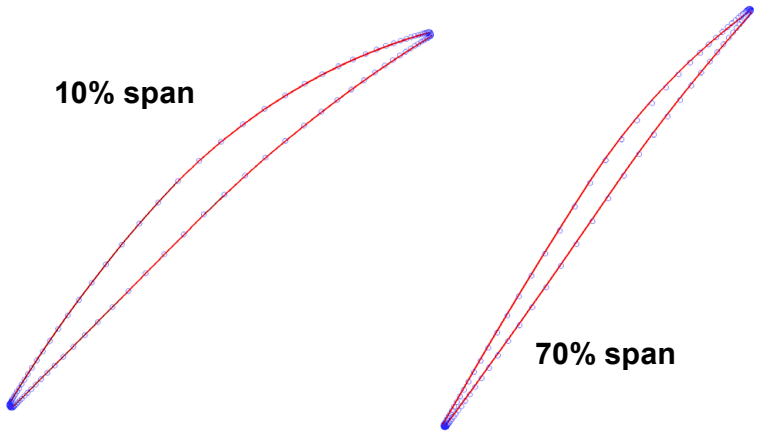

Figure 13 Comparison of original (red lines) and recovered (blue circles) geometry

Table 2 Performance comparison of original and recovered geometries

	Mass flow [kg/s]	*total pressure ratio [-]*	*adiabatic efficiency [-]*
original	*20.95*	*2.071*	*0.890*
recovery	*20.96*	*2.069*	*0.891*

4 Conclusions

A reformulation of a three-dimensional inverse design method has been presented. This method does not use special inverse boundary conditions and velocity tracing to modify the blade camber. Instead, camber modification is performed using a blade velocity derived from the difference between prescribed and existing pressure loading. The existing pressure loading is obtained from the flow solution. Differences between analysis and inverse calculations are completely eliminated. It is also fully consistent with viscous flow modelling in that the flow velocity at the blade wall can be zero.

The effectiveness and robustness of the new method is demonstrated through a redesign and subsequent recovery of the original geometry and performance of NASA Rotor 37, a highly loaded transonic rotor with separated flow present along the entire span starting at approximately 75% chord.

The reformulated inverse method effectively decouples the inverse method from the flow solver. This makes it possible to supplement any CFD-code with the developed inverse design module, provided the possibility exists for an interface between the solver and the inverse module through which to pass flow and mesh information. This includes most commercial CFD-software, which makes inverse design available to most design offices.

5 References

[1] Hield, P., "Semi-Inverse Design Applied to an Eight Stage Transonic Axial Flow Compressor", ASME Paper GT2008-50430.

[2] Daneshkhah, K., and Ghaly, W., 2006, "An Inverse Blade Design Method for Subsonic and Transonic Viscous Flow in Compressors and Turbines," Inverse Probl. Sci. Eng., 14, no. 3, pp. 211–231.

[3] Mileshin, V., Orekhov, I., Shchipin, S., and Startsev, A., 2007, "3D Inverse Design of Transonic Fan Rotors Efficient for a Wide Range of RPM," ASME Paper No. GT2007-27817.

[4] Dang, T.Q., 1995, "Inverse Method for Turbomachine Blades Using Shock-Capturing Techniques," AIAA Paper 95–2465.

[5] Damle, S., Dang, T., Stringham, J., and Razinsky, E., 1999, "Practical Use of a 3D Viscous Inverse Method for the Design of Compressor Blade," ASME Journal of Turbomachinery, 121, no. 2, pp. 321-325.

[6] Medd, A.J., Dang, T.Q., and Larosiliere, L.M., 2003, "3D Inverse Design Loading Strategy for Transonic Axial Compressor Blading," ASME Paper 2003-GT-38501.

[7] Van Rooij, M. P. C., Dang, T. Q., and Larosiliere, L. M., 2007, "Improving aerodynamic matching of axial compressor blading using a three-dimensional multistage inverse design method". ASME Journal of Turbomachinery, 129, no. 1, pp. 108–118.

[8] Van Rooij, M.P.C., Dang, T.Q. and Larosiliere, L.M., 2008,"Enhanced Blade Row Matching Capabilities via 3D Multistage Inverse Design and Pressure Loading Manager", ASME Paper 2008-GT-50539.

[9] Ji, M., Dang, T.Q., and Cave, M.J., "Fully Three-Dimensional Viscous Semi-Inverse Method for Subsonic Mixed-Flow and Radial Impeller Design", ASME Paper GT2009-59679.

[10] Qiu, X., Ji, M. and Dang, T., 2009, "Three-Dimensional Viscous Inverse Method for Axial Blade Design", Inverse Problems in Science and Engineering, 17, no. 8, pp. 1019-1036

[11] Larosiliere, L.M., Wood, J.R., Hathaway, M.D., Medd, A. J., and Dang, T.Q., 2002, "Aerodynamic Design Study of an Advanced Multistage Axial Compressor," NASA TP–211568.

[12] Jameson, A., Schmidt, W., and Turkel, E., 1981, "Numerical Solution of the Euler Equations by Finite Volume Methods Using Runge-Kutta Time-Stepping Schemes," AIAA Paper 81–1259.

[13] Radespiel, R., Rossow, C., and Swanson, R. C., 1990. “Efficient Cell-Vertex Multigrid Scheme for the Three-Dimensional Navier-Stokes Equations”. AIAA Journal, 28(8), pp. 1464–1472.

[14] Piegl, L., and Miller, W., 1997, “The NURBS Book”, Springer, Berlin.

[15] Hall, E.J. and Delaney, R.A., 1995, “Investigation of Advanced Counterrotation Blade Configuration Concepts for High Speed Turboprop Systems: Task VII-ADPAC User’s Manual,” NASA CR–195472.

[16] Denton, J.D., 1997, “Lesson from Rotor 37”, Journal of Thermal Science, Vol. 6, No. 1.

[17] Chima, R.V., 2009, “SWIFT Code Assessment for Two Similar Transonic Compressors”, NASA/TM-2009-215520 and Paper AIAA-2009-1058.

[18] Ameri, A. A., 2009, “NASA Rotor 37 CFD Code Validation Glenn-HT Code”, Paper AIAA 2009-1060.

[19] Shabbir, A., Celestina, M.L., Adamczyk, J.J. and Strazisar, A.J., 1997, “The Effect of Hub Clearance Flow on Two High Speed Axial Flow Compressor Rotors”, ASME paper 97-GT-346

[20] Chandra, R., Dagum, L., Kohr, D., Maydan, D., McDonald, J. and Menon, R., 2001, “Parallel programming in OpenMP”, 2001, Morgan Kaufmann Publishers Inc. San Francisco, CA, USA.